Shell Thickness Dependent Photoinduced Hole Transfer in Hybrid Conjugated Polymer/Quantum Dot Nanocomposites: From Ensemble to Single Hybrid Level

Zhihua Xu,[†] Corey R. Hine,[‡] Mathew M. Maye,[‡] Qingping Meng,[†] and Mircea Cotlet[†,*]

[†]Brookhaven National Laboratory, Upton, New York 11973, United States and [‡]Department of Chemistry, Syracuse University, Syracuse, New York 13224, United States

ABSTRACT

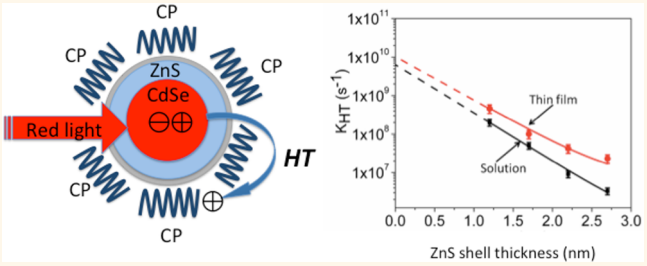

Photoinduced hole transfer is investigated in inorganic/organic hybrid nanocomposites of colloidal CdSe/ZnS quantum dots and a cationic conjugated polymer, poly(9,9′-bis(6-*N*,*N*,*N*-trimethylammoniumhexyl)fluorene-alt-phenylene, in solution and in solid thin film, and down to the single hybrid level and is assessed to be a dynamic quenching process. We demonstrate control of hole transfer rate in these quantum dot/conjugated polymer hybrids by using a series of core/shell quantum dots with varying shell thickness, for which a clear exponential dependency of the hole transfer rate *vs* shell thickness is observed, for both solution and thin-film situations. Furthermore, we observe an increase of hole-transfer rate from solution to film and correlate this with changes in quantum dot/polymer interfacial morphology affecting the hole transfer rate, namely, the donor–acceptor distance. Single particle spectroscopy experiments reveal fluctuating dynamics of hole transfer at the single conjugated polymer/quantum dot interface and an increased heterogeneity in the hole-transfer rate with the increase of the quantum dot's shell thickness. Although hole transfer quenches the photoluminescence intensity of quantum dots, it causes little or no effect on their blinking behavior over the time scales probed here.

KEYWORDS: photoinduced hole transfer · hybrid inorganic/organic · quantum dots · conjugated polymers · single-molecule spectroscopy · optoelectronics

Semiconducting organic/inorganic nanocomposites are appealing optoelectronic materials due to the possibility of combining desired properties from both components in one, thus creating new properties that may not be present in each individual material. In particular, blends of conjugated polymers (CPs) and semiconductor quantum dots (QDs) have attracted interest for applications such as light-emitting diodes (LEDs),[1−4] photovoltaics (PV),[5−8] and biosensing.[9] The interaction between the excited states of a CP and a QD, which determines the optoelectronic properties of the resulting hybrid material, needs to be fully understood. The highest occupied molecular orbital (HOMO) and the lowest unoccupied molecular orbital (LUMO) of the CP and QD in such hybrids is usually of type II alignment, thus facilitating both charge separation and energy transfer between components under light exposure. Specifically, charge separation can be achieved by either electron transfer from the photoexited CP to the QD or by hole transfer (HT) from the photoexcited QD to the CP. When both the CP and QD are photoexcited, all three types of interactions may compete in a single hybrid, thus leading to a complicated photoresponse. For example, both energy transfer and charge separation have been observed between CdSe QDs and their conjugated ligands.[10,11] Energy transfer between CP and QD has been investigated, and both Förster- and Dexter-type mechanisms have been proposed.[12−16] Photoinduced electron transfer from CP to QD has also been intensively investigated, along with the increased interest in the utilization of such organic/inorganic hybrids in PV applications.[17−20] Hole transfer from QD to CP on the other hand remains little explored and understood. Hole transfer from QD to CP is an essential process in achieving high power conversion efficiency in PV cells, but a detrimental process for applications such as LEDs and biosensing. Although working PV cells based on CP/QD hybrids prove indirectly the presence of hole transfer, to our knowledge, there exists only one report on hole transfer in solution from InP QDs to conjugated poly(3-hexylthiophene).[21] Better design of new hybrids for optoelectronic and biosensory applications requires a systematic study of

* Address correspondence to cotlet@bnl.gov.

Received for review February 5, 2012 and accepted June 1, 2012.

Published online June 11, 2012
10.1021/nn300525b

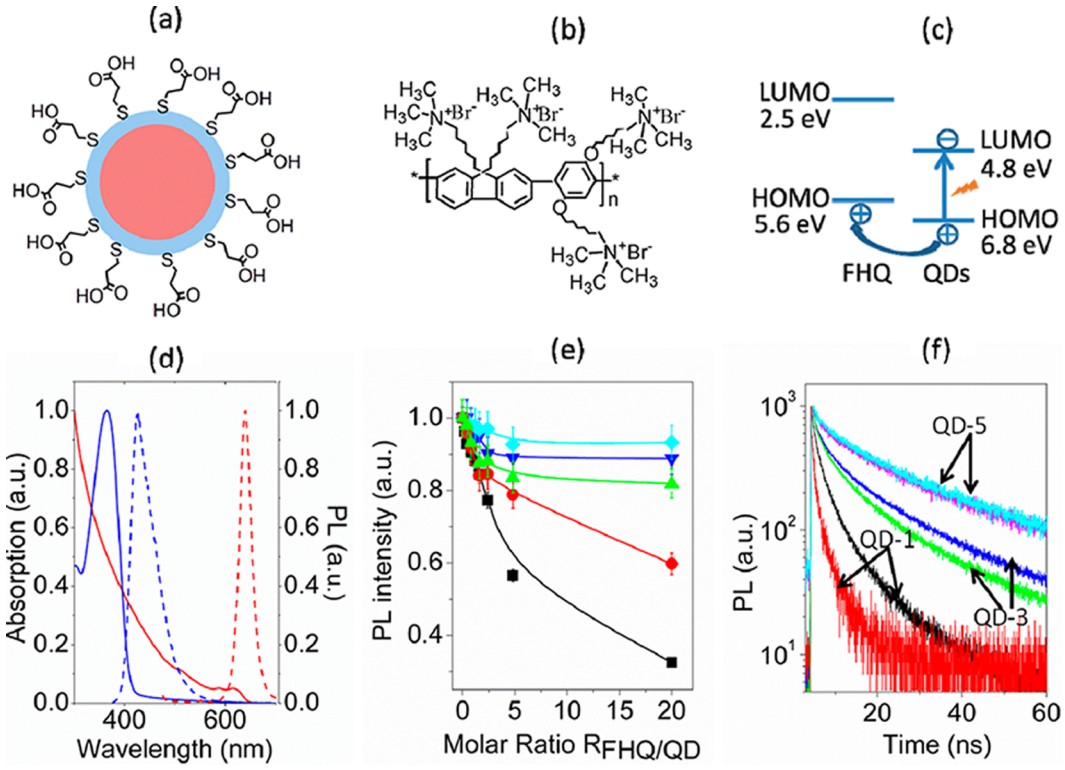

Figure 1. (a) MPA-capped core/shell CdSe/ZnS quantum dots (QDs) and (b) cationic conjugated polymer FHQ (adapted from ref 22). (c) Scheme for photoinduced hole transfer between QD and FHQ. (d) UV (solid) and PL (dash) spectra of QD-1 (red) and FHQ (blue) in aqueous solution. (e) PL intensity *vs* FHQ/QD molar ratio, $R_{FHQ/QD}$, for hybrids based on QD-1 (black square), QD-2 (red dots), QD-3 (green triangles), QD-4 (blue triangles), and QD-5 (magenta rhombs). (f) transient PL decays of QD-1 (black) and FHQ/QD-1 ($R_{FHQ/QD}$ = 20, red) of QD-3 (green) and FHQ/QD-3($R_{FHQ/QD}$ = 20, blue) and of QD-5 (cyan) and FHQ/QD-5 ($R_{FHQ/QD}$ = 20, magenta).

hole transfer in CP/QD hybrids. For example, the development of PV and LED devices based on CP/QD thin films invokes more interest in the characterization of hole transfer in solid films rather than in solution. Similarly, biosensors utilizing CP/QD hybrids can benefit in sensitivity if one can understand how hole transfer affects QDs' emission properties.

Here, we investigate photoinduced hole transfer from a CdSe/ZnS core/shell QD with varying shell thickness (Figure 1a) to a water-soluble conjugated polymer, poly(9,9′-bis(6-*N*,*N*,*N*-trimethylammoniumhexyl)-fluorene-alt-phenylene[22] (FHQ, MW ~15 kDa) (Figure 1b). For this particular donor/acceptor hybrid, the emission peaks of FHQ (450 nm) and QD (634−638 nm) are well separated, enabling the selective excitation of only the QD in a hybrid, for example by exciting with 590 nm light, so that HT from photoexcited QD to CP is probed exclusively by monitoring the steady-state and transient photoluminescence (PL) decay from the QD. In the present work, we investigate photoinduced HT in the FHQ/QD composite both in solution and in solid thin films by ensemble-based PL measurement. Furthermore, we use single-particle spectroscopy to probe the dynamics of HT and to resolve the heterogeneity of HT at a single CP/QD interface and to probe the effect of HT on the photoluminescence blinking dynamics of QDs.

RESULTS AND DISCUSSION

A series of five 3-mercaptopropionic acid (MPA)-capped CdSe/ZnS QDs were synthesized with average shell thicknesses of 1.2 nm (QD-1), 1.7 nm (QD-2), 2.2 nm (QD-3), 2.7 nm (QD-4), and 4.2 nm (QD-5), respectively (see Table S1, Supporting Information (SI), for structural and photophysical parameters). These are negatively charged water-soluble QDs that are expected to electrostatically bind cationic FHQ[22] and to form a stable organic/inorganic nanocomposite.[23] Indeed, dynamic light scattering (DLS) measurements clearly show a size increase from QDs-only to QDs blended with FHQ (see Figure S2, SI), thus confirming the electrostatical binding of the two components in solution. Assuming that the ZnS shell acts as a tunneling barrier for hole transfer from the photoexcited QD to FHQ, this series of QDs can be used to probe and at the same time to demonstrate distance-dependent photoinduced HT in CP/QD hybrids. TEM images of QDs together with the corresponding size distribution analysis are provided in the SI (Figure S1), and they were used to estimate the QD's core size and shell thickness. With increased shell thickness, the PL peak of the QDs slightly shifts from 634 nm (QD-1, QD-2) to 635 nm (QD-3, QD-4) and to 638 nm (QD-5), and the PL quantum yield increases from 7% (QD-1) to as high as 25% (QD-5) and so does the PL

lifetime (Table S1, SI). The shell thickness dependency for both PL quantum yield and PL lifetime for QDs is consistent with published reports that suggest increased leakage of the exciton wave function into the shell and improved passivation of surface defects with increasing the shell thickness.[24−26]

Hole Transfer in Solution. We probed hole transfer in solution by blending QDs (200 nM in borate buffer) with FHQ at various FHQ/QD molar ratios (denoted $R_{FHQ/QD}$), from 0:1 to 20:1, and by measuring the PL intensity and PL lifetime at the emission peak of the QD (λ_{exc} = 590 nm). At a molar ratio $R_{FHQ/QD} \approx$ 20, one expects that all QDs have bound conjugated polymer FHQ. As expected, the strongest PL quenching was observed for the FHQ/QD-1 hybrid, with QD-1 having the thinnest ZnS shell (1.2 nm, see Figure 1e, f). At the highest polymer concentration ($R_{FHQ/QD\text{-}1}$ = 20), the PL intensity of the FHQ/QD-1 hybrid is quenched 67% (Figure 1e) and the corresponding PL lifetime is quenched 62% (Figure 1f). This suggests efficient electrostatic binding of the conjugated polymer FHQ to the surface of the QD and also dynamic quenching of the QD's photoluminescence by hole transfer to FHQ. Indeed, MPA-capped QDs and cationic FHQ are expected to form a stable hybrid due to electrostatic interaction between the negatively charged MPA linker and positively charged side chains of FHQ, and this is also demonstrated by DLS measurements (Figure S2, SI). Furthermore, the dynamic PL quenching of QDs by hole transfer to FHQ is a result of the presence of the ZnS shell acting as an additional tunneling barrier for HT. This is in contrast to a previous report on the HT in solution in InP QD/P3HT hybrids.[21] In that particular case, significant changes in the PL intensity of InP core-only QDs due to hole transfer to P3HT were accompanied by very little change in the related PL lifetime, supposedly because not all QDs would bind to P3HT to form hybrids. Only those QDs that were complexed with P3HT experienced complete PL quenching by efficient HT. CdSe/ZnS QDs with thicker shells also experience dynamic PL quenching, although somewhat less dramatic: for the same $R_{FHQ/QD}$ = 20 molar ratio, the estimated PL quenching is 40% for FHQ/QD-2, 18% for FHQ/QD-3, 11% for FHQ/QD-4, and 7% for FHQ/QD-5 (Figure 1e). PL decays of QD-1, QD-3, and QD-5 and of their corresponding FHQ/QD hybrids are shown in Figure 1f.

Let us assume that the average PL lifetimes of QDs and FHQ/QD hybrids are given by $\tau_{QD} = 1/(k_R + k_{NR})$ and $\tau_{FHQ/QD} = 1/(k_R + k_{NR} + k_{HT})$, respectively, with k_R and k_{NR} being radiative and nonradiative rates for QD, respectively, and k_{HT} being the rate for HT from photoexcited QD to FHQ. k_{HT} can be calculated as

$$k_{HT} = 1/\tau_{FHQ/QD} - 1/\tau_{QD} \quad (1)$$

Applying eq 1 to the PL lifetime data from Figure 1f gives an estimated rate $k_{HT} \approx 2.0 \times 10^8$ s^{-1} for FHQ/QD-1 in solution ($R_{FHQ/QD\text{-}1}$ = 20), that is, the hybrid exhibiting the strongest PL quenching. According to the charge-transfer theory, the rate for charge transfer is given by

$$k_{HT} \propto \frac{4\pi^2}{h}(H^2)\frac{1}{(4\pi\lambda k_B T)^{1/2}}\exp\left(-\frac{(\Delta G^0+\lambda)^2}{4\pi\lambda k_B T}\right) \quad (2)$$

with H being electronic coupling, ΔG^0 the free energy, and λ the reorganization energy. ΔG^0 is determined by the HOMO and LUMO levels of the donor and acceptor components (Figure 1c), while H is determined by the overlap between the hole wave function in the QD and the HOMO of FHQ, which is a function of donor−acceptor separation distance. Assuming the HOMO and LUMO of both components remain unchanged when changing only the ZnS shell thickness (denoted here as t_s), the rate k_{HT} for FHQ/QD hybrids should be sensitive only to changes in donor−acceptor separation distance, in this case the ZnS shell thickness, t_s, by

$$k_{HT} = k_0 \exp(-\beta t_s) \quad (3)$$

with β being a damping factor. A fit of k_{HT} *vs* ZnS shell thickness by eq 3 yields a damping factor $\beta \approx 2.8$ nm^{-1} (see Figure 2, black line), hence confirming the tunneling barrier character for the ZnS shell against the hole transfer from QD to FHQ. The value of the damping factor β in the FHQ/QD hybrid is comparable to that reported for CdSe/CdS core/shell nanorods adsorbed with small-molecule hole acceptors such as phenothiazine (PTZ) ($\beta \approx 4.0$).[27] Extrapolation of the dependency k_{HT} *vs* ZnS shell thickness t_s from Figure 2 to zero shell thickness renders a rate $k_{HT}(0) \approx 5.2 \times 10^9$ s^{-1} for the hole transfer between CdSe core-only and FHQ in solution, which is similar to that reported for CdSe core-only QDs adsorbed with PTZ molecules.[28]

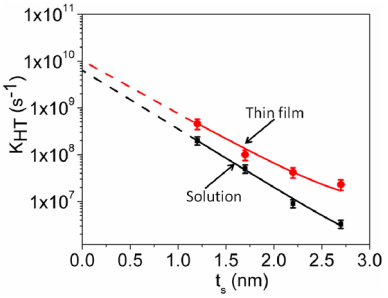

Figure 2. Shell thickness (t_s) *vs* HT rate (k_{HT}) dependency for FHQ/QD blended solutions (black squares) and thin films (red dots). Fits according to eq 3 (solid lines).

Hole Transfer in Concentrated Thin Films. We next investigated FHQ/QD hybrid solid thin films ($R_{FHQ/QD}$ = 20) and bare QDs spin-casted on a glass surface and studied them with confocal fluorescence lifetime imaging microscopy (FLIM) (Figure 3). Both FHQ/QD hybrid and bare QD thin-film samples were prepared from solutions of similar QD concentration (200 nM). Bare QDs on a glass surface exhibit average PL lifetimes

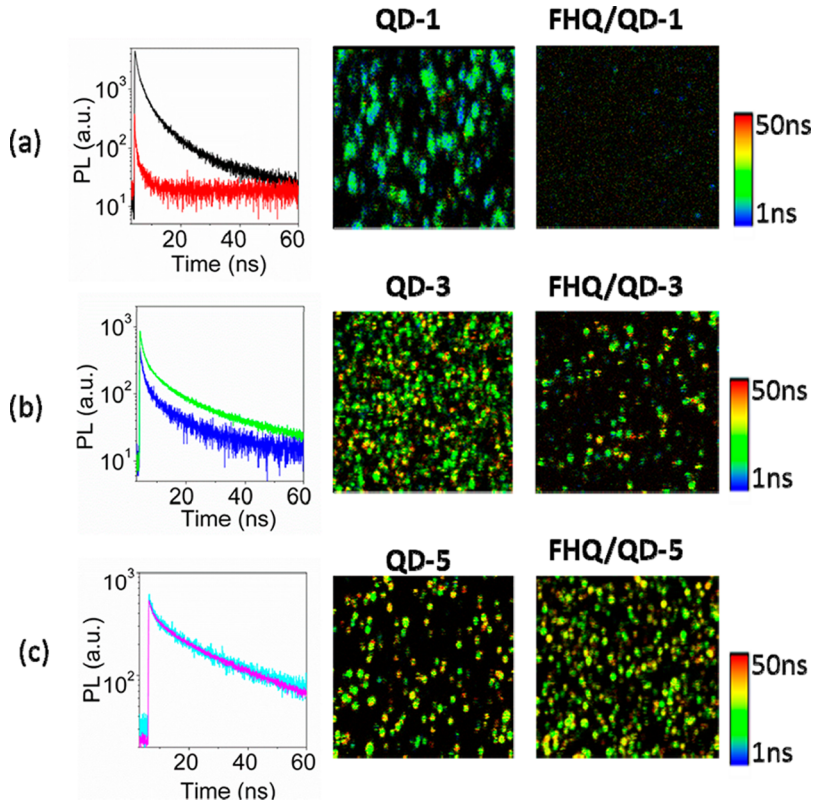

Figure 3. HT in concentrated FHQ/QD thin films. Left: Average PL decays from (a) QD-1 on surface (black) and FHQ/QD-1 hybrid thin films (red), from (b) QD-3 on surface (green) and FHQ/QD-3 hybrid thin films (blue), and from (c) QD-5 on surface (cyan) and FHQ/QD-3 thin films (magenta). Right: FLIM images (15 × 15 μm) of QD on surface and of FHQ/QD hybrid thin films for (a) QD-1, (b) QD-3, and (c) QD-5.

similar to those observed in solution (see Figure 3a–c; PL decays in left panels, FLIM images in center panels). FHQ/QD hybrids exhibit quenched PL lifetimes, except for FHQ/QD-5 hybrids, which incorporate QDs with the thickest ZnS shell (4.2 nm) (see Figure 3a–c; PL decays in left panels, FLIM images in right panels). Using eq 1, we calculated an average rate for HT between QD-1 and FHQ in solid thin films of k_{HT}(FHQ/QD-1) ≈ 4.6 × 10^8 s^{-1}, with the FHQ/QD-1 hybrid expected to exhibit the strongest hole transfer. Similarly, we calculated k_{HT} for hybrids incorporating QD-2, QD-3, and QD-4 to find that the rate for HT for FHQ/QD hybrids in thin-films also scales exponentially with the ZnS shell thickness (see Figure 2), and with a damping factor $\beta \approx 2.7$ nm^{-1}, similar to the solution case. Extrapolation of the exponential dependency from Figure 2 to zero ZnS shell thickness renders a limiting rate $k_{HT}(0) \approx 1.1 \times 10^{10}$ s^{-1} for the HT from the CdSe core-only QD to FHQ polymer for solid thin films. It is noteworthy that FHQ/QD hybrids exhibit more significantly quenched PL lifetimes in thin films than in solution, suggesting increased HT efficiency in the former case. This observation is true for each of the investigated QDs (*e.g.*, QD-1 to QD-4), and it is also shown by the k_{HT} *vs* t_s dependencies from Figure 2. This enhancement in the HT rate from solution to thin films can be attributed primarily to a denser packing of the conjugated polymer chains on the QD's surface in the case of solid thin films, which in turn increases the electronic coupling between the donor and acceptor components. A change in the driving force for hole transfer from solution to solid thin film resulting from changes in FHQ band gap and/or dielectric environment might result in enhanced HT in the former case.

To further investigate the tunneling barrier character of the ZnS shell on the HT rate, we used the effective mass theory to estimate the CdSe hole wave function density at the surface of the ZnS shell in the QDs.[25,26] In this model, QDs are treated as particles confined in spherical wells of finite depth. For calculation purposes we used valence band edges for the CdSe core and ZnS shell of −6.8 and −7.4 eV, respectively,[29] a HOMO level of −6.7 eV,[30] and a layer thickness of 1 nm for MPA ligands and effective masses for holes in CdSe and ZnS of 0.45 and 1.3, respectively.[26] In the calculations, the Schrodinger equation for the QD system is solved numerically to obtain the hole wave function distribution in the core/shell structure. For example, the radial probability function obtained for the 1S hole wave function in a QD with a 12 Å ZnS shell thickness is shown in Figure S3a (SI). The density of the hole wave function at the surface of the ZnS shell *vs* shell thickness t_s is shown in Figure S3b, and it decays exponentially with a damping factor of 7.3 nm^{-1}. Since the rate for HT is proportional to the electronic coupling (*H*)

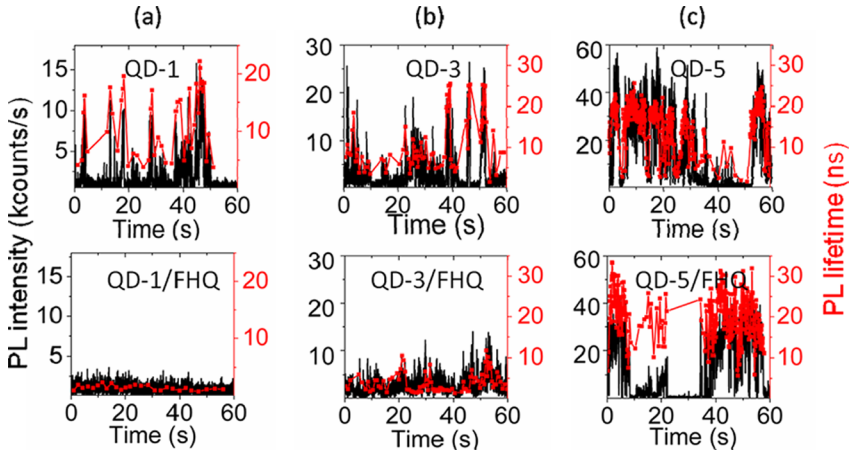

Figure 4. Time trajectories of PL intensity (black line) and PL lifetime (red line and squares) for isolated QDs (upper panel) and FHQ/QD-1 hybrids (lower panel): (a) QD-1 and FHQ/QD-1; (b) QD-3 and FHQ/QD-3; (c) QD-5 and FHQ/QD-5.

between the CdSe hole wave function and the HOMO of FHQ (see eq 2), it should scale with the hole density at the shell surface and therefore depend exponentially on the ZnS shell thickenss. The relatively small discrepancy between the values of the damping factors obtained experimentally for the hole-transfer rate and theoretically for the hole wave function density may be related to the inhomogenity of ZnS shell coating. This speculation is supported by the relatively low PL quantum yield and by the multiexponential decay of the PL of these QDs (see Table S1 and Figure 1f), which are indicative of the existence of large amounts of surface defects, and this is further addressed below. It is noteworthy that the MPA surface ligands play a role in enhancing hole transfer in the FHQ/QD hybrid system. Our calculations show that the high HOMO level of MPA ligands increase the hole wave function density at the QD surface (see Figure S3a), consistent with previous reports where similar ligands to MPA, for example thiols, act as hole acceptors for CdSe QDs.[30,31]

Hole Transfer in Single FHQ/QD Hybrids. We next performed single-particle PL spectroscopy on diluted samples of isolated QDs and of FHQ/QD thin film blends spin-casted on cover glass. Antibunching experiments were also performed to ensure that the detected signal was indeed from isolated QDs or FHQ/QD hybrids (see Figure S4, SI). Typical PL intensity and lifetime trajectories recorded from isolated QD-1, QD-3, and QD-5 and from their corresponding hybrids, FHQ/QD-1, FHQ/QD-3, and FHQ/QD-5, are shown in Figure 4a–c. They demonstrate the effect of ZnS shell thickness on the HT at the single FHQ/QD hybrid level: from thin (1.2 nm for QD-1, Figure 4a) to intermediate (2.2 nm for QD-3, Figure 4b), to thick shell (4.2 nm, QD-5, Figure 4c), hole transfer quenches the PL intensity and lifetime in hybrids from very efficient (FHQ/QD-1, Figure 4a) to intermediate (FHQ/QD-3, Figure 4b), to negligible (FHQ/QD-5, Figure 4c). Due to efficient HT in the case of the FHQ/QD-1 hybrid, very few isolated FHQ/QD-1 hybrids are "visible" by single-particle spectroscopy and the PL signal from such hybrids is too weak to render reliable statistical analysis (see Figure 4a, lower panel). Due to the negligible HT in FHQ/QD-5 hybrids, we noticed no significant difference between PL signals from isolated QD-5 and FHQ/QD-5 hybrids (Figure 4c). QD-2, QD-3, and QD-4, nanocrystals with intermediate shell thickness, and their related hybrids displayed decent PL signals for reliable statistical analysis, so they were considered for the discussion of HT at the single hybrid level.

The speculation of inhomogeneous coating of the CdSe core by the ZnS shell is further supported by the dynamics of the PL intensity and lifetime observed in single-particle experiments. For example, for isolated QD-3 (2.2 nm shell thickness), the PL intensity exhibits random fluctuations with a wide distribution of on-states (Figure 4b, upper panel), different from the well-known "telegraph-like" blinking signal.[32] The PL lifetimes for an isolated QD-3 show correlated fluctuations with the PL intensity (Figure 4b), suggesting a fluctuating nonradiative recombination rate for photogenerated excitons. Similar "nontelegraphic" PL blinking was observed previously for isolated QDs and attributed to photoiduced electron trapping on the QD's surface or in external defects[33,34] and for QDs coupled to a fullerene acting as an external electron trap.[35] Therefore, the nontelegraphic PL blinking of isolated QD-3 could be related to inhomogeneous coating of the CdSe core by the ZnS layer, here inducing the coupling of the photogenerated excitons with the surface defects in the core/shell QDs. The same behavior could also be related to structual defects induced by large lattice mismatch between CdSe and ZnS, which creates nonradiative recombination sites.[25,36] For isolated FHQ/QD hybrids, HT becomes an additional quenching pathway for the excited state of the QD, since both the PL intensity and PL lifetime for the hybrid are quenched when compared to the isolated QD

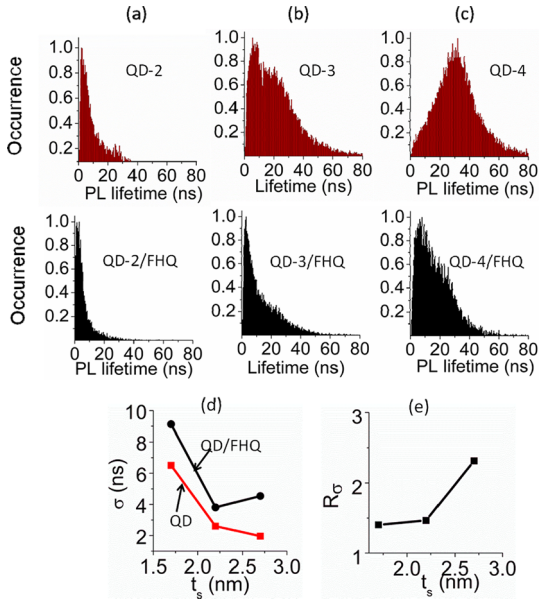

Figure 5. Distributions of PL lifetimes for isolated QDs (upper panels, red color) and isolated FHQ/QD hybrids (lower panels, black color): (a) QD-2 and FHQ/QD-2; (b) QD3 and FHQ/QD-3; (c) QD4 and FHQ/QD-4. (d) Standard deviation (σ) of PL lifetime *vs* ZnS shell thickness, t_s, for the distributions shown in panels (a)–(c) (black line and dots, FHQ/QD, red line and squares, QD). (e) Ratio (R_σ) of standard deviations of PL lifetime for FHQ/QD hybrids and for QDs *vs* ZnS shell thickness, t_s.

(Figure 4a–b). Furthermore, both the PL intensity and PL lifetime for isolated FHQ/QD hybrids exhibit quasi-continuous on-states (Figure 4b, lower panel), indicating a fluctuating HT rate at the single-particle level, similar to previous single-molecule reports on electron transfer between QDs and different acceptors[35,37–39] or other organic molecules.[40–44]

In order to characterize the degree of fluctuation of the HT rate in single FHQ/QD hybrids, we constructed distributions of PL lifetimes from 50 randomly selected isolated nanoparticles of each category, QD-2, QD-3, QD-4 (Figure 5, upper panels), and their FHQ/QD related isolated hybrids (Figure 5, lower panels). The heterogeneity in PL lifetime and therefore in the rate for HT was assessed by the standard deviation σ,

$$\sigma(\tau) = \sqrt{\frac{1}{N}\sum_{i=1}^{N}(\tau_i - \tau_{av})^2} \qquad (4)$$

with N being the number of PL lifetime events contributing to a distribution, τ_i the PL lifetime of event i, and τ_{av} the average lifetime calculated here as $\tau_{av} = 1/N\sum\tau_i$. With the increase in ZnS shell thickness, from QD-2 to QD-3 and to QD-4, PL lifetime distributions shift to larger values (Figure 5a–c), consistent with the ensemble solution and thin-film data (Figures 2 and 3). At the same time, σ becomes smaller with the increase of ZnS shell thickness (Figure 5d, red line and squares), indicating a reduced fluctuation in the nonradiative recombination rate for photogenerated excitons in QDs. It is

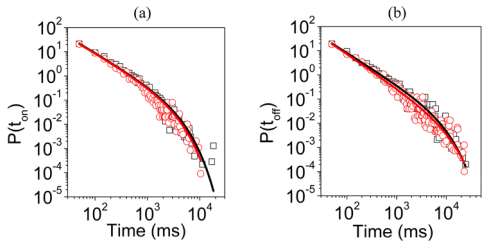

Figure 6. Probability distributions $P(t_{on})$, (a) and $P(t_{off})$, (b) for QD-3 (black squares) and FHQ/QD-3 hybrids (red dots). Fits according to eq 5 (solid lines): For QD-3 (black curves), $P(t_{on})$ has $m_{on} = 1.3$ and $t_{on} = 2.8$ s; $P(t_{off})$ has $m_{off} = 1.3$ and $t_{off} = 6.6$ s. For FHQ/QD-3 (red curves), $P(t_{on})$ has $m_{on} = 1.3$ and $t_{on} = 2.5$ s; $P(t_{off})$ has $m_{off} = 1.4$ and $t_{off} = 8.3$ s.

largely accepted that an increase in the shell thickness leads to a reduced density of surface traps.[24–26] Therefore, the data from Figure 5d and pertaining to isolated QDs further support our previous speculation that fluctuations in the PL lifetime and PL intensity of isolated QDs are strongly dependent on the density of surface traps, which here are determined by the ZnS shell inhomogeneity. Coupling of a QD with the FHQ polymer significantly increases the heterogeneity in the measured PL lifetimes, as the standard deviation σ increases considerably for any given ZnS thickness (Figure 5d, black line and dots). Consequently, HT induces additional heterogeneity (fluctuation) into the exciton decay rate of a QD when this is part of a FHQ/QD hybrid. The contribution of HT to the overall fluctuation present in a FHQ/QD hybrid can be retrieved by plotting the ratio R_σ of standard deviations for single FHQ/QD hybrids and for isolated QDs *vs* shell thickness (Figure 5e). Surprisingly, R_σ increases with the increase of ZnS shell thickness, suggesting an increase in the degree of fluctuation in HT for thicker shells, contrary to the way the rate for HT behaves. One possible explanation for such observed behavior is given below. An increase in the QD's shell thickness leads to a larger surface area that can complex with the FHQ polymer. In other words, a QD with a thicker ZnS shell can couple more polymer chains, and meanwhile it can possess a larger degree of variation in surface coupling, which indubitably induces a larger static and dynamic heterogeneity in the PL lifetime when HT is present.

We next address the effect of hole transfer on the PL blinking dynamics of QDs. PL blinking of isolated QDs, or the switching of their emitted PL between bright (on) and dark (off) states, has been related to photo-induced charging of the QD core:[32] a QD will stay bright (on-state) when the core is neutral and the photogenerated eletron–hole recombine radiatively or will become dark (off-state) when the core is charged and efficient Auger recombination overwhelms the radiative pathway. This model has been widely used to explain the PL blinking phenomenon of quantum dots, although recent experimental observations and theortical models have proposed the existence of additional blinking mechanisms.[45–49] PL blinking dynamics

for isolated QDs is often characterized by the distributions of the on-times, $P(t_{on})$, and off-times, $P(t_{off})$, with t_{on} and t_{off} defined by a threshold value, here for example set at three times the standard deviation over the average background signal.[50] $P(t_{on})$ and $P(t_{off})$ distributions corresponding to isolated QD-3 and FHQ/QD-3 are shown in Figure 6, and those corresponding to isolated QD-2, FHQ/QD-2 and QD-4, and FHQ/QD-4 are shown in the SI in Figure S5. Each of these distributions contains data extracted from 50 randomly selected PL intensity traces of equal time (here 60 s each). For isolated QD-2, QD-3, and QD-4, the $P(t_{off})$ and $P(t_{on})$ distributions are well fitted with a truncated power-law function described by[51−53]

$$P(t) = bt^{-m} \exp\left(-\frac{t}{\tau}\right) \quad (5)$$

with m being the power law exponent and τ the cross-over time from power law to exponential decay behavior. Similar blinking behavior of isolated QDs has been observed previously by us[53] and by others[51,52] and associated with the presence of surface trap charges (defects) inducing additional nonradiative recombination and thus affecting QD blinking dynamics. $P(t_{off})$ and $P(t_{on})$ distributions for FHQ/QD hybrids can also be fitted well with eq 5 (Figure 6 and Figure S5), and they do not differ significantly from those corresponding to isolated QDs, thus indicating a trivial effect of HT on the QD's blinking dynamics at the time scale we probed (from 20 ms to 20 s). This is in sharp contrast with the effect of electron transfer on the QDs' blinking dynamics observed in the case of QDs coupled with electron acceptors such as fullerenes[35,37] or titanium oxide,[38] where photoinduced electron transfer was found to reduce t_{on}. In the present case, when a QD forms a complex with FHQ, hole transfer clearly emerges as an additional pathway competing with radiative recombination, as it is demonstrated by the observed quenched PL intensity and PL lifetime (see Figure 4), two observables that are associated with the on-states of the QD. The on-states for FHQ/QD (Figure 4b) resemble the gray states of isolated QDs proposed in a few references.[54,55] On the other hand, hole transfer is expected to affect the dynamics of Auger recombination and of other nonradiative recombinations by regulating the charging and discharging processes of the QD core and, hence, affecting the PL blinking dynamics. However, we observed no significant effect of HT on the blinking dynamics of QDs at time scales longer than 20 ms, a binning time we were forced to use in order to obtain trustworthy data for the blinking analysis. This suggests the necessity to probe blinking dynamics in the presence of HT at an even shorter time scale and to compare this with the effect of electron transfer on the same process.

CONCLUSION

In summary, photoinduced hole transfer in hybrids based on CdSe/ZnS QDs and the cationic conjugated polymer FHQ has been investigated in solution and solid film and down to the single-particle level. The HT rate in FHQ/QD hybrids exhibits clear exponential dependency on the thickness of the ZnS shell, providing the tunneling barrier character of the shell toward HT. In addition, the rate is found to be larger in solid films than in solution, suggesting a significant effect of interfacial morphology on the HT. Single-particle spectroscopy not only confirms the shell thickness dependency observed in ensemble measurements, but also reveals the fluctuating dynamics of HT at the single FHQ/QD interface. From the analysis of distributions of PL lifetimes of isolated hybrids, the heterogeneity of HT is found to increase with the thickness of the ZnS shell. Although HT quenches the intensity of the on-states of quantum dots, it shows little effect on their on-time and off-time distributions at long time scale as probed here.

MATERIALS AND METHODS

Materials. Details on the synthesis of MPA-capped CdSe/ZnS QDs and FHQ polymer are given in the SI. Blends of FHQ/QD were prepared from a 200 nM borate-buffered solution of QDs by adding FHQ at various molar ratios. For concentrated thin films, blended solutions were spin-casted on precleaned cover-glasses. For single-particle experiments, blended solutions were diluted (1000×) and spin-casted on precleaned cover-glasses to ensure a concentration of 1 QD/μm^2 or less. For diluted QD-only samples, QDs were spin-casted directly on the precleaned cover-glass. For both concentrated thin films and single-particle experiments, samples were purged with nitrogen prior to (20 min) and during the measurement.

Microscopy. Ensemble PL lifetimes, FLIM, and single-particle fluorescence microscopy measurements were performed on a home-built confocal scanning stage microscope based on an inverted microscope (Olympus IX81, 1.4 NA 100× oil objective) equipped with a piezo scanning stage (Physik Instrumente, Germany) and coupled to a diode-pumped solid-state laser system delivering 590 nm pulses of 250 fs width, at 8 MHz repetition rate (Spectra Physics, Newport). The average power at the sample was kept at about 100 nW. The fluorescence was collected in epi-illumination format, spectrally separated from the excitation laser light by a dichroic (Semrock, DiO-594) and by a band-pass filter (Semrock FF01-628/40), and detected by a single photon counting avalanche photodiode (APD, MPD Picoquant) and a time-analyzer (PicoHarp 300, PicoQuant). For single-particle spectroscopy, fluorescence was split (50/50) by a nonpolarizing beam spliter cube and detected by two APDs to allow for antibunching measurements (see details in the SI). Data acquisition and data analysis were performed with the Symphotime analysis software (Picoquant). Dynamic light scattering experiments were performed on a commercial Malvern Zetasizer NS.

Conflict of Interest: The authors declare no competing financial interest.

Acknowledgment. Research was carried out in part at the Center for Functional Nanomaterials of Brookhaven National Laboratory in Upton, New York, under the Office of Science US-DOE Contract No. DE-AC02-98CH10886. M.M.M. thanks the AFOSR

(FA9550-10-1-0033) and ACS-PRF (51303-DNI10) for financial support. We thank Dr. H. L. Wang from Los Alamos National Laboratory in New Mexico and Dr. Jongwook Park from Catholic University of Korea, Dr. H. Y. Woo from Pusan National University in South Korea for providing the conjugated polymer, Dr. Arindam Chakraborty from Syracuse University and Dr. Mark Hybertsen from Brookhaven National Laboratory for help with theoretical interpretation of some data, and Dr. D. Sun for help with DLS experiments.

Supporting Information Available: Details on colloidal quantum dot synthesis, core size and shell thickness estimation by TEM, and the corresponding size distribution analysis. Structural and photophysical data on QDs with varying shell thickness, details on antibunching experiments, and antibunching data on isolated QDs and FHQ/QD hybrids, distributions of on- and off-times for isolated QD-2, FHQ/QD-2 and QD-4, FHQ/QD-4. Details on theoretical estmation of hole transfer rate, including the calculation of the 1S hole wave function in CdSe/ZnS QD and hole wave function density at ZnS surface *vs* ZnS shell thickness. This material is available free of charge *via* the Internet at http://pubs.acs.org.

REFERENCES AND NOTES

1. Colvin, V. L.; Schlamp, M. C.; Alivisatos, A. P. Light-Emitting-Diodes Made from Cadmium Selenide Nanocrystals and a Semiconducting Polymer. *Nature* **1994**, *370*, 354–357.
2. Dabbousi, B. O.; Bawendi, M. G.; Onitsuka, O.; Rubner, M. F. Electroluminescence from Cdse Quantum-Dot Polymer Composites. *Appl. Phys. Lett.* **1995**, *66*, 1316–1318.
3. Tessler, N.; Medvedev, V.; Kazes, M.; Kan, S. H.; Banin, U. Efficient Near-Infrared Polymer Nanocrystal Light-Emitting Diodes. *Science* **2002**, *295*, 1506–1508.
4. Koktysh, D. S.; Gaponik, N.; Reufer, M.; Crewett, J.; Scherf, U.; Eychmuller, A.; Lupton, J. M.; Rogach, A. L.; Feldmann, J. Near-Infrared Electroluminescence From HgTe Nanocrystals. *ChemPhysChem* **2004**, *5*, 1435–1438.
5. Huynh, W. U.; Dittmer, J. J.; Alivisatos, A. P. Hybrid Nanorod-Polymer Solar Cells. *Science* **2002**, *295*, 2425–2427.
6. Campbell, I. H.; Crone, B. K. Quantum-Dot/Organic Semiconductor Composites for Radiation Detection. *Adv. Mater.* **2006**, *18*, 77–79.
7. McDonald, S. A.; Konstantatos, G.; Zhang, S. G.; Cyr, P. W.; Klem, E. J. D.; Levina, L.; Sargent, E. H. Solution-Processed PbS Quantum Dot Infrared Photodetectors And Photovoltaics. *Nat. Mater.* **2005**, *4*, 138–U14.
8. Thelakkat, M.; Maria, S.; Susha, A. S.; Sommer, M.; Talapin, D. V.; Rogach, A. L. Semiconductor Block Copolymer Nanocomposites with Lamellar Morphology *via* Self-Organization. *Macromolecules* **2008**, *41*, 6081–6088.
9. Rogach, A. L.; Jiang, G. X.; Susha, A. S.; Lutich, A. A.; Stefani, F. D.; Feldmann, J. Cascaded FRET in Conjugated Polymer/Quantum Dot/Dye-Labeled DNA Complexes for DNA Hybridization Detection. *ACS Nano* **2009**, *3*, 4127–4131.
10. Early, K. T.; Sudeep, P. K.; Emrick, T.; Barnes, M. D. Polarization-Driven Stark Shifts in Quantum Dot Luminescence from Single CdSe/oligo-PPV Nanoparticles. *Nano Lett* **2010**, *10*, 1754–1758.
11. Odoi, M. Y.; Hammer, N. I.; Sill, K.; Emrick, T.; Barnes, M. D. Observation of Enhanced Energy Transfer In Individual Quantum Dot-Oligophenylene Vinylene Nanostructures. *J. Am. Chem. Soc.* **2006**, *128*, 3506–3507.
12. Anni, M.; Manna, L.; Cingolani, R.; Valerini, D.; Creti, A.; Lomascolo, M. Forster Energy Transfer From Blue-Emitting Polymers to Colloidal Cdse/Zns Core Shell Quantum Dots. *Appl. Phys. Lett.* **2004**, *85*, 4169–4171.
13. Chang, T. W. F.; Musikhin, S.; Bakueva, L.; Levina, L.; Hines, M. A.; Cyr, P. W.; Sargent, E. H. Efficient Excitation Transfer from Polymer to Nanocrystals. *Appl. Phys. Lett.* **2004**, *84*, 4295–4297.
14. Mahrt, R. F.; Kaufmann, S.; Stoferle, T.; Moll, N.; Scherf, U.; Tsami, A.; Talapin, D. V.; Murray, C. B.: Resonant Energy Transfer within a Colloidal Nanocrystal Polymer Host System. *Appl. Phys. Lett.* **2007**, *90*.
15. Mahrt, R. F.; Stoferle, T.; Scherf, U. Energy Transfer in Hybrid Organic/Inorganic Nanocomposites. *Nano Lett.* **2009**, *9*, 453–456.
16. Stefani, F. D.; Lutich, A. A.; Jiang, G.; Susha, A. S.; Rogach, A. L.; Feldmann, J. Energy Transfer *versus* Charge Separation in Type-II Hybrid Organic-Inorganic Nanocomposites. *Nano Lett* **2009**, *9*, 2636–2640.
17. Greenham, N. C.; Peng, X. G.; Alivisatos, A. P. Charge Separation and Transport in Conjugated-Polymer/Semiconductor-Nanocrystal Composites Studied by Photoluminescence Quenching and Photoconductivity. *Phys. Rev. B* **1996**, *54*, 17628–17637.
18. Ginger, D. S.; Greenham, N. C. Photoinduced Electron Transfer from Conjugated Polymers to CdSe Nanocrystals. *Phys. Rev. B* **1999**, *59*, 10622–10629.
19. Lin, Z. Q.; Xu, J.; Wang, J.; Mitchell, M.; Mukherjee, P.; Jeffries-EL, M.; Petrich, J. W. Organic-Inorganic Nanocomposites *via* Directly Grafting Conjugated Polymers onto Quantum Dots. *J. Am. Chem. Soc.* **2007**, *129*, 12828–12833.
20. Heinemann, M. D.; von Maydell, K.; Zutz, F.; Kolny-Olesiak, J.; Borchert, H.; Riedel, I.; Parisi, J. Photo-induced Charge Transfer and Relaxation of Persistent Charge Carriers in Polymer/N anocrystal Composites for Applications in Hybrid Solar Cells. *Adv. Funct. Mater.* **2009**, *19*, 3788–3795.
21. Selmarten, D.; Jones, M.; Rumbles, G.; Yu, P. R.; Nedeljkovic, J.; Shaheen, S. Quenching of Semiconductor Quantum Dot Photoluminescence by a Pi-Conjugated Polymer. *J. Phys. Chem. B* **2005**, *109*, 15927–15932.
22. Kang, M.; Nag, O. K.; Nayak, R. R.; Hwang, S.; Suh, H.; Woo, H. Y. Signal Amplification by Changing Counterions in Conjugated Polyelectrolyte-Based FRET DNA Detection. *Macromolecules* **2009**, *42*, 2708–2714.
23. Mayya, K. S.; Schoeler, B.; Caruso, F. Preparation and Organization of Nanoscale Polyelectrolyte-Coated Gold Nanoparticles. *Adv. Funct. Mater.* **2003**, *13*, 183–188.
24. Hines, M. A.; Guyot-Sionnest, P. Synthesis and Characterization of Strongly Luminescing Zns-Capped CdSe Nanocrystals. *J. Phys. Chem.-US* **1996**, *100*, 468–471.
25. Dabbousi, B. O.; RodriguezViejo, J.; Mikulec, F. V.; Heine, J. R.; Mattoussi, H.; Ober, R.; Jensen, K. F.; Bawendi, M. G. (CdSe)ZnS Core-Shell Quantum Dots: Synthesis and Characterization of a Size Series Of Highly Luminescent Nanocrystallites. *J. Phys. Chem. B* **1997**, *101*, 9463–9475.
26. Zhu, H. M.; Song, N. H.; Lian, T. Q. Controlling Charge Separation and Recombination Rates in CdSe/ZnS Type I Core-Shell Quantum Dots by Shell Thicknesses. *J. Am. Chem. Soc.* **2010**, *132*, 15038–15045.
27. Jiang, Z. J.; Kelley, D. F.; Leppert, V. Static and Dynamic Emission Quenching in Core/Shell Nanorod Quantum Dots with Hole Acceptors. *J. Phys. Chem. C* **2009**, *113*, 19161–19171.
28. Huang, J. E.; Huang, Z. Q.; Jin, S. Y.; Lian, T. Q. Exciton Dissociation in CdSe Quantum Dots by Hole Transfer to Phenothiazine. *J. Phys. Chem. C* **2008**, *112*, 19734–19738.
29. Hummon, M. R.; Stollenwerk, A. J.; Narayanamurti, V.; Anikeeva, P. O.; Panzer, M. J.; Wood, V.; Bulovic, V. Measuring Charge Trap Occupation and Energy Level in Cdse/Zns Quantum Dots Using a Scanning Tunneling Microscope. *Phys. Rev. B* **2010**, 81.
30. Ning, Z. J.; Molnar, M.; Chen, Y.; Friberg, P.; Gan, L. M.; Agren, H.; Fu, Y. Role of Surface Ligands in Optical Properties of Colloidal CdSe/CdS Quantum Dots. *Phys. Chem. Chem. Phys.* **2011**, *13*, 5848–5854.
31. Wuister, S. F.; Donega, C. D.; Meijerink, A. Influence of Thiol Capping on the Exciton Luminescence and Decay Kinetics of CdTe and CdSe Quantum Dots. *J. Phys. Chem. B* **2004**, *108*, 17393–17397.
32. Efros, A. L.; Rosen, M. Random Telegraph Signal in the Photoluminescence Intensity of a Single Quantum Dot. *Phys. Rev. Lett.* **1997**, *78*, 1110–1113.
33. Schlegel, G.; Bohnenberger, J.; Potapova, I.; Mews, A. Fluorescence Decay Time of Single Semiconductor Nanocrystals. *Phys. Rev. Lett.* **2002**, *88*.
34. Zhang, K.; Chang, H. Y.; Fu, A. H.; Alivisatos, A. P.; Yang, H. Continuous Distribution of Emission States From Single CdSe/ZnS Quantum Dots. *Nano Lett.* **2006**, *6*, 843–847.
35. Xu, Z. H.; Cotlet, M. Quantum Dot-Bridge-Fullerene Heterodimers with Controlled Photoinduced Electron Transfer. *Angew. Chem. Int. Ed.* **2011**, *50*, 6079–6083.

36. Baranov, A. V.; Rakovich, Y. P.; Donegan, J. F.; Perova, T. S.; Moore, R. A.; Talapin, D. V.; Rogach, A. L.; Masumoto, Y.; Nabiev, I. Effect of ZnS Shell Thickness on the Phonon Spectra in CdSe Quantum Dots. *Phys. Rev. B* **2003**, *68*.
37. Song, N. H.; Zhu, H. M.; Jin, S. Y.; Zhan, W.; Lian, T. Q. Poisson-Distributed Electron-Transfer Dynamics from Single Quantum Dots to C60 Molecules. *ACS Nano* **2011**, *5*, 613–621.
38. Jin, S. Y.; Lian, T. Q. Electron Transfer Dynamics from Single CdSe/ZnS Quantum Dots to TiO_2 Nanoparticles. *Nano Lett* **2009**, *9*, 2448–2454.
39. Issac, A.; Jin, S. Y.; Lian, T. Q. Intermittent Electron Transfer Activity from Single CdSe/ZnS Quantum Dots. *J. Am. Chem. Soc.* **2008**, *130*, 11280–11281.
40. Biju, V.; Micic, M.; Hu, D. H.; Lu, H. P. Intermittent Single-Molecule Interfacial Electron Transfer Dynamics. *J. Am. Chem. Soc.* **2004**, *126*, 9374–9381.
41. Wang, Y. M.; Wang, X. F.; Ghosh, S. K.; Lu, H. P. Probing Single-Molecule Interfacial Electron Transfer Dynamics of Porphyrin on TiO_2 Nanoparticles. *J. Am. Chem. Soc.* **2009**, *131*, 1479–1487.
42. Cotlet, M.; Masuo, S.; Lor, M.; Fron, E.; Van der Auweraer, M.; Mullen, K.; Hofkens, J.; De Schryver, F. Probing the Influence O-2 on Photoinduced Reversible Electron Transfer in Perylenediimide-Triphenylamine-Based Dendrimers by Single-Molecule Spectroscopy. *Angew. Chem., Int. Ed.* **2004**, *43*, 6116–6120.
43. Bell, T. D. M.; Stefan, A.; Masuo, S.; Vosch, T.; Lor, M.; Cotlet, M.; Hofkens, J.; Bernhardt, S.; Mullen, K.; van der Auweraer, M.; Verhoeven, J. W.; De Schryver, F. C. Electron Transfer at the Single-Molecule Level in a Triphenylamine-Perylene Imide Molecule. *ChemPhysChem* **2005**, *6*, 942–948.
44. Cotlet, M.; Masuo, S.; Luo, G. B.; Hofkens, J.; Van der Auweraer, M.; Verhoeven, J.; Mullen, K.; Xie, X. L. S.; De Schryver, F. Probing Conformational Dynamics in Single Donor-Acceptor Synthetic Molecules by Means of Photoinduced Reversible Electron Transfer. *Proc. Natl. Acad. Sci. U. S. A.* **2004**, *101*, 14343–14348.
45. Jha, P. P.; Guyot-Sionnest, P. Trion Decay in Colloidal Quantum Dots. *ACS Nano* **2009**, *3*, 1011–1015.
46. Zhao, J.; Nair, G.; Fisher, B. R.; Bawendi, M. G. Challenge to the Charging Model of Semiconductor-Nanocrystal Fluorescence Intermittency from Off-State Quantum Yields and Multiexciton Blinking. *Phys. Rev. Lett.* **2010**, *104*, 157403.
47. Rosen, S.; Schwartz, O.; Oron, D. Transient Fluorescence of the Off State in Blinking CdSe/CdS/ZnS Semiconductor Nanocrystals Is Not Governed by Auger Recombination. *Phys. Rev. Lett.* **2010**, *104*, 157404.
48. Frantsuzov, P. A.; Marcus, R. A. Explanation of Quantum Dot Blinking without the Long-Lived Trap Hypothesis. *Phys. Rev. B* **2005**, *72*, 155321.
49. Galland, C.; Ghosh, Y.; Steinbruck, A.; Sykora, M.; Hollingsworth, J. A.; Klimov, V. I.; Htoon, H. Two Types of Luminescence Blinking Revealed by Spectroelectrochemistry of Single Quantum Dots. *Nature* **2011**, *479*, 203–U75.
50. Kuno, M.; Fromm, D. P.; Hamann, H. F.; Gallagher, A.; Nesbitt, D. J. Nonexponential "Blinking" Kinetics of Single CdSe Quantum Dots: A Universal Power Law Behavior. *J. Chem. Phys.* **2000**, *112*, 3117–3120.
51. Drndic, M.; Wang, S.; Querner, C.; Emmons, T.; Crouch, C. H. Fluorescence Blinking Statistics from CdSe Core and Core/Shell Nanorods. *J. Phys. Chem. B* **2006**, *110*, 23221–23227.
52. Peterson, J. J.; Nesbitt, D. J. Modified Power Law Behavior in Quantum Dot Blinking: A Novel Role for Biexcitons and Auger Ionization. *Nano Lett.* **2009**, *9*, 338–345.
53. Xu, Z.; Cotlet, M Photoluminescence Blinking Dynamics of Colloidal Quantum Dots in the Presence of Controlled External Electron Traps. *Small* **2012**, *8*, 253–258.
54. Spinicelli, P.; Buil, S.; Quelin, X.; Mahler, B.; Dubertret, B.; Hermier, J. P. Bright and Grey States in CdSe-CdS Nanocrystals Exhibiting Strongly Reduced Blinking. *Phys. Rev. Lett.* **2009**, *102*.
55. Kipp, T.; Ma, X. D.; Tan, H.; Mews, A. Fluorescence Enhancement, Blinking Suppression, and Gray States of Individual Semiconductor Nanocrystals Close to Gold Nanoparticles. *Nano Lett.* **2010**, *10*, 4166–4174.